J. Plasma Phys. (2019), *vol.* 85, 905850509
doi:10.1017/S0022377819000655

Volumetric measurement of the synchronization and desynchronization of the dust acoustic wave with an external modulation

Jeremiah D. Williams†

Department of Physics, Wittenberg University, Springfield, OH 45504, USA

(Received 10 June 2019; revised 9 September 2019; accepted 10 September 2019)

A spatio-temporal measurement showing the volumetric nature of the phase synchronization of a naturally occurring dust acoustic wave to an external modulation and the relaxation from the driven wave mode back to the naturally occurring wave mode (phase desynchronization) is presented. It is shown that the phase synchronization and desynchronization occur behind a propagating synchronization/desynchronization front that travels at a slower speed than the phase velocity of the wave and that the speed of this synchronization/desynchronization front decreases with increasing neutral gas pressure. It is also observed that volume of the wave that is synchronous depends on the frequency of the external modulation and the neutral gas pressure.

Key words: complex plasmas, dusty plasmas, plasma nonlinear phenomena

1. Introduction

Nanometre to micrometre sized particulate matter (dust) is often observed to be embedded in both naturally occurring and laboratory produced plasmas. These dust grains become charged through interactions with the electrons and ions in the background plasma. The resulting plasma system consists of three charged species and is notably more complex than the traditional plasma system due to the interactions between the charged dust with the other plasma components (i.e. the ions and electrons). The presence of this third charged species self-consistently alters the properties of the surrounding plasma medium and results in a system that supports a wide range of new plasma phenomena, including a low-frequency, longitudinal wave mode that propagates through the dust component known as the dust acoustic (or dust density) wave that is self-excited by the free energy from the ions streaming through the dust component (Merlino 2014).

Experimentally, these dusty plasma systems are attractive because the dust grains are large enough to be directly observed and the (relatively) small charge to mass ratio of dust results in characteristic time scales for the dust phenomena that are of the order of $\sim$10 s of Hz. As a result, these systems are relatively easy to access experimentally with the use of diagnostic tools as simple as a video imaging. This allows for the study of the properties of the dust-related phenomena such as the dust

† Email address for correspondence: jwilliams@wittenberg.edu

acoustic wave mode at both the global and individual particle level with incredible spatial and temporal resolution (Killer & Melzer 2014; Tadsen *et al.* 2015; Tadsen, Greiner & Piel 2017; Yaroshenko *et al.* 2019). In recent years, this has allowed for the study of a wide range of the properties this wave mode, including wave–particle interactions (Liao *et al.* 2008; Chang, Teng & Lin 2012), the growth (Thomas 2006; Flanagan & Goree 2011; Heinrich *et al.* 2011; Williams 2013) and dispersion relation (Trottenberg, Block & Piel 2006; Thomas, Fisher & Merlino 2007; Rosenberg, Thomas & Merlino 2008; Nosenko *et al.* 2009; Williams & Snipes 2010; Ruhunusiri & Goree 2014; Avinash 2015; Davletov *et al.* 2018) of this wave mode, wave breaking (Liao *et al.* 2008; Teng *et al.* 2009) and turbulence (Tsai, Chang & Lin 2014). Further, the majority of the experimental observations that have been made of this wave mode in the laboratory setting involve waves that are nonlinear (Merlino 2012). This has allowed for the detailed study of the nonlinear properties (Liu *et al.* 2018) of this wave mode and of related nonlinear processes. One type of nonlinear process that has been studied is phase synchronization (Pikovsky, Rosenblum & Kurths 2001), a process that is ubiquitous in a variety of plasma and physical systems and plays an important role in many self-organized phenomena (Tass *et al.* 1998; Maza *et al.* 2000; Ticos *et al.* 2000; Rosenblum, Pikovsky & Kurths 2004). In the context of dusty plasmas and the dust acoustic wave, phase synchronization occurs when the naturally occurring dust acoustic wave mode couples with and adjusts to an externally applied modulation (Pilch, Reichstein & Piel 2009; Ruhunusiri & Goree 2012; Williams 2014*b*, 2018*a*).

In a previous work, a preliminary measurement depicting the time-resolved, volumetric nature of the phase synchronization of the naturally occurring dust acoustic wave with an externally applied modulation in a radio frequency (rf) discharge was reported (Williams 2018*b*). In that work, it was observed that the volume of the cloud that is synchronous depends on the modulation frequency. In this paper, we present a systematic study of the volumetric nature of the phase synchronization and desynchronization of the naturally occurring dust acoustic wave with an externally applied modulation in a rf discharge as a function of neutral gas pressure and modulation frequency with the experimental procedure being described in § 2, the analysis technique being described in § 3 and results being presented in § 4.

2. Experimental procedure

The experiments presented here were performed in the Wittenberg University DUsty Plasma DEvice (WUDUPE), figure 1, where a rf discharge argon plasma was generated using a pair of electrodes. The 8.3 cm (3.25 in.) diameter upper electrode is powered using a 13.56 MHz, rf generator. The lower electrode, a rectangular block of size 7.6 × 17.8 cm (3 × 7 in.), is positioned ∼6 cm (2.4 in) below the upper electrode and is connected to a high voltage power supply that is biased with respect to the grounded vacuum chamber wall, V_b, to allow for control of the current that is drawn to the lower electrode, I_{elec}. This lower electrode is also loaded with 1.0 μm silica microspheres ($\rho = 2000$ kg m^{-3}), which serve as the source dust for these experiments (Williams & Snipes 2010; Williams 2018*a*).

Once the plasma has been initiated, the dust particles acquire a net negative charge from the background plasma and are lifted from the lower electrode into the discharge over the course of several minutes to form a large, stable dust cloud between the two electrodes. Here, the dust is confined by the gravitational and electrical forces due to the self-consistently formed potential structure of the powered electrode.

https://doi.org/10.1017/S0022377819000655 Published online by Cambridge University Press

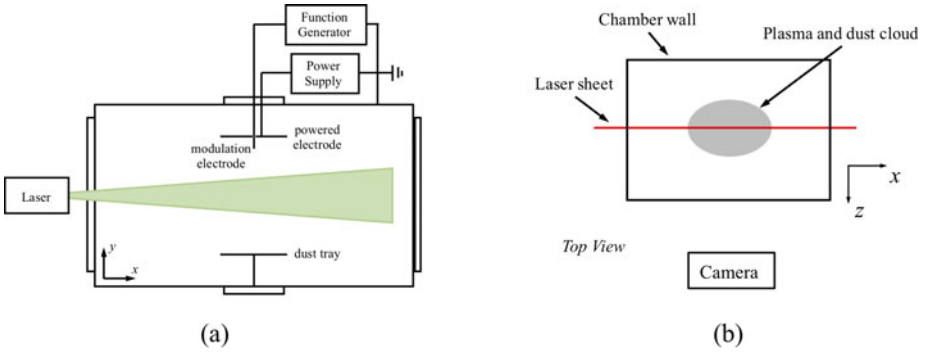

FIGURE 1. (*a*) Sketch of the experimental apparatus. The dust clouds examined here form between the powered (upper) electrode and the lower electrode that holds the dust for the experiments presented. (*b*) Top view of the experimental set-up showing the orientation of the laser sheet and camera used in the experiments presented here.

Once a stable cloud has been formed, the experimental parameters are adjusted until a self-excited dust acoustic wave is observed to spontaneously appear and propagate in the $-y$-direction, i.e. parallel to the direction of gravity. For the measurements reported here, the wave was observed to exists throughout the measured volume of the cloud. The experimental conditions were then further adjusted until the behaviour of the wave is observed to be modified by the application of a sinusoidally varying voltage to a tungsten wire (modulation) electrode ($l = 3$ mm, $d = 0.5$ mm) positioned approximately $\sim$1.0 cm above the dust cloud. The minimum voltage necessary to synchronize the wave mode to this external modulation was applied to the modulation electrode over the range of frequencies reported in table 1, which represents the range of frequency over which phase synchronization was observed. This frequency range was broken into five equal steps and each frequency was applied sequentially for 3.0 s with a 1.0 s gap between each applied frequency. The first frequency was applied 0.5 s after the camera began recording data. The triggering of the camera and the application of the external modulation were controlled by a LabVIEW program to provide reproducibility. The experimental parameters examined here are listed table 1. The plasma parameters were measured with a Langmuir probe when dust was not present.

To observe the dynamics of the wave, the dust particles were illuminated using a 200 mW diode pumped solid state laser ($\lambda = 532$ nm) whose output was expanded into a $\sim$1 mm thick vertical light sheet. Video sequences of approximately 5400 images were acquired at a rate of 250 frames per second using a Photron SA3 CMOS camera as the various modulation frequencies were applied to the modulation electrode. The camera was positioned perpendicular to the laser sheet and was equipped with a band pass filter to eliminate light emitted by the background plasma glow. The volumetric nature of the phase synchronization process was measured by moving the laser and camera, which were fixed relative to each other, through the cloud in 3 mm steps covering the volume of the cloud where phase synchronization was observed and was optically accessible.

3. Analysis technique

From the image data, the spatio-temporal evolution of the phase and the dominant frequency of the observed wave mode are obtained by applying a time-resolved

https://doi.org/10.1017/S0022377819000655 Published online by Cambridge University Press

p (mTorr)	p_{rf} (W)	V_b (V)	I_{elec} (mA)	n_e (m^3)	T_e (eV)	f (Hz)	v_{ph} (mm s^{-1})
60	2.5	−94.7	−0.53	$(8.7 \pm 0.1) \times 10^{14}$	3.4 ± 0.2	17–33	65.5 ± 0.5
76	2.5	−94.5	−0.44	$(1.1 \pm 0.1) \times 10^{15}$	2.9 ± 0.3	20–36	52.5 ± 0.8
90	2.45	−54.8	−0.31	$(1.4 \pm 0.2) \times 10^{15}$	3.3 ± 0.4	20–40	40.4 ± 0.6
106	2.4	−55.7	−0.23	$(8.9 \pm 0.1) \times 10^{14}$	2.8 ± 0.1	22–38	38.5 ± 0.7

TABLE 1. Experimental parameters.

Hilbert transform technique to the acquired image sequence previously described (Menzel, Arp & Piel 2011*b*; Williams 2014*a*). Briefly, the wave structure as a function of time at each pixel in the acquired images, $n_d(x, y, t)$, is found by extracting the image intensity after applying a Gaussian low-pass filter to each image to suppress the effects of the granularity of individual particles and subtracting the time averaged background dust density, $n_{d,o}$, from each filtered image. The analytic signal, $A(x, y, t)$, is then constructed by expanding the measured wave structure into the complex plane using (3.1)

$$A(x, y, t) = n_d(x, y, t) + \imath \hat{n}_d(x, y, t) = E(x, y, t) \exp[\mathrm{i} \cdot \phi(x, y, t)], \tag{3.1}$$

where $\hat{n}_d(x, y, t)$ is the Hilbert transform of the measured wave structure, $E(x, y, t) = \sqrt{n_d^2 + \hat{n}_d^2}$ is the amplitude and $\phi(x, y, t) = \text{atan2}[\hat{n}_d(x, y, t), n_d(x, y, t)]$ is the instantaneous phase of the wave mode. The instantaneous phase is then unwrapped to eliminate discontinuities due to phase jumps from $2\pi \rightarrow 0$. The same process is then applied to the external modulation. To fully examine the onset and loss of phase synchronization, the signal that represents the external modulation was modified so that the duration of each modulation frequency was extended to last for 4.0 s with no gap between each drive frequency used. This extension of the modulation signal in the analysis process allows for the examination of the loss of phase synchronization once the modulation has been discontinued. The difference in the unwrapped phase between the wave and the external modulation is then used to determine if the wave is synchronous with the external modulation. The degree of synchronization between the phase of the wave mode and the phase of the external modulation is quantified using the synchronization index, equation (3.2) (Couëdel *et al.* 2014; Williams 2014*b*).

$$\gamma = \frac{H_{\max} - H}{H_{\max}}. \tag{3.2}$$

This index provides a statistical measure of the strength of the phase synchronization using the Shannon entropy, $H = \sum_{k=1}^{N} p_k \ln(p_k)$, where p_k is the fraction of data in the kth bin in the distribution of the cumulative difference in the unwrapped phase, $N = 20$ is the number of bins used to construct the distribution of the cumulative difference in the unwrapped phase and $H_{\max} = \ln(N)$ is the maximum entropy corresponding to a uniform distribution. The distribution of the difference in phases is then constructed using a rolling window having a length of 101 consecutive frames centred on time t. The synchronization index scales between 0 (desynchronized) and 1(fully synchronization), providing a measure of the degree of phase synchronization between the wave mode and the external modulation. In the literature, phase synchronization is indicated by plateaus of elevated values of the synchronization index, γ (Tass *et al.* 1998). In this work, the wave is identified as being synchronous with the external modulation if the mean value of the synchronization index exceeds a nominal value of 0.3 for a period of 0.2 s.

https://doi.org/10.1017/S0022377819000655 Published online by Cambridge University Press

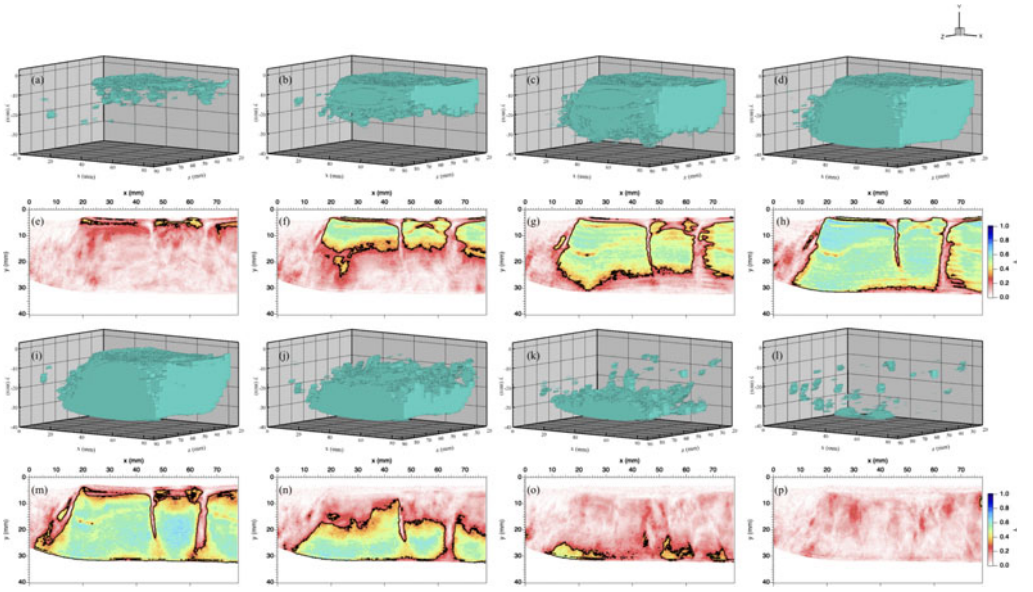

FIGURE 2. Isosurfaces depicting the volume of the wave mode that is synchronous after the (*a–d*) onset and (*i–l*) discontinuation of an external modulation of $f = 28$ at $p = 76$ mTorr. Plots showing the synchronization index and synchronized region (black contours) at these time steps in the dust cloud directly under the modulation electrode after the (*e–h*) onset and (*m–p*) discontinuation of an external modulation. The source of the external modulation is located at $(x, z) = (54.94, 39.00)$ mm and the time between the panels in is 0.2 s.

4. Experimental results

In observing the phase synchronization of the naturally occurring wave mode with an external modulation, it was observed that either the majority of wave volume or a small volume of wave in the region directly below modulation electrode became synchronous with the external modulation; consistent with previously reported observations (Williams 2014*b*, 2018*a*,*b*). Two representative measurements depicting the types of behaviour that was observed as the naturally occurring wave mode became synchronous at the onset of the external modulation are seen in figures 2 ($p = 76$ mTorr, $f_{\mathrm{mod}} = 28$ Hz) and 3 ($p = 106$ mTorr, $f_{\mathrm{mod}} = 22$ Hz). For reference, the modulation electrode is positioned at $(x, y, z) = (54.94, 1.06, 39)$ mm for the data seen in figure 2 and positioned at $(x, y, z) = (53.97, 2.60, 39)$ mm for the data seen in figure 3. Here, the plotted isosurfaces depict the region of the wave that is synchronous at the (*a–d*) onset and (*i–l*) following the discontinuation of the external modulation in time steps of 200 ms, with (*a*,*e*) being 0.1 s after the initiation of the external modulation and (*i*,*m*) being 0.02 s after the discontinuation of the external modulation. The values of the synchronization index at these time steps in the imaged slice of the dust cloud directly under the modulation electrode during the onset and discontinuation of the external modulation are seen in (*e–h*) and (*m–p*), respectively. The contour depicts the region of cloud that is synchronous with the external modulation.

In both cases, the upper region of the cloud nearest the modulation electrode initially becomes synchronous with the external modulation shortly after the initiation

https://doi.org/10.1017/S0022377819000655 Published online by Cambridge University Press

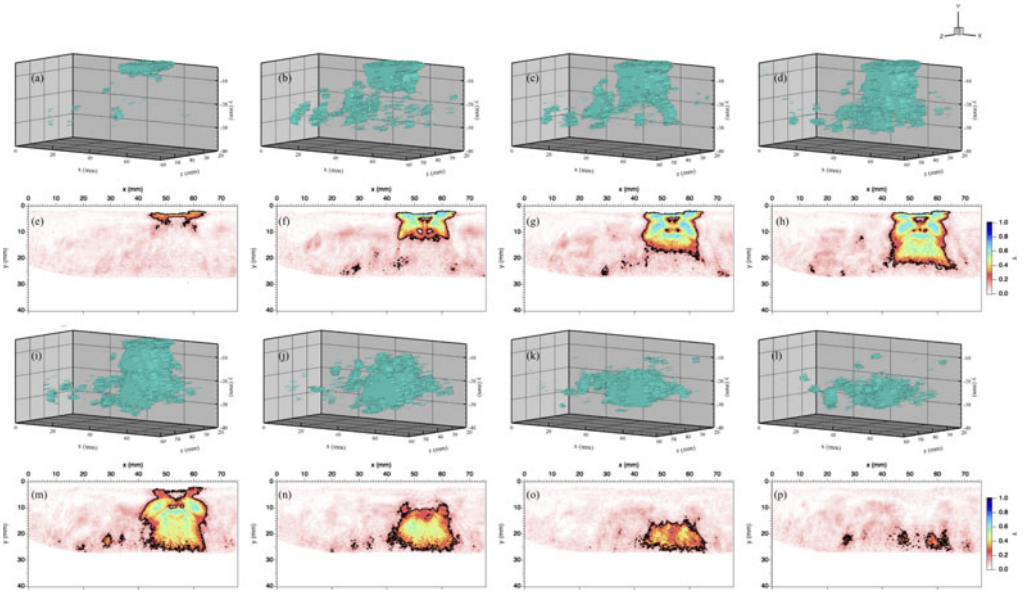

FIGURE 3. Isosurfaces depicting the volume of the wave mode that is synchronous after the (*a–d*) onset and (*i–l*) discontinuation of an external modulation of $f = 22$ at $p = 106$ mTorr. Plots showing the synchronization index and synchronized region (black contours) at these time steps in the dust cloud directly under the modulation electrode after the (*e–h*) onset and (*m–p*) discontinuation of an external modulation. The source of the external modulation is located at $(x, z) = (53.97, 39.00)$ mm and the time between the panels in is 0.2 s.

of the external modulation, figures 2, 3(*a–h*). As this happens, it is observed that the spacing of the wave fronts becomes regular in the upper region of the cloud and that the dominant frequency mode in the upper region of the cloud adjusts to match the frequency of the external modulation. As time passes, the region of the cloud exhibiting the characteristics that are associated with the driven mode expands to fill the cloud, consistent with previously reported observations (Williams 2014*b*, 2018*a*). Additionally, phase synchronization is observed to happen behind a propagating synchronization front that travels at a slower speed than the phase velocity of the wave, as previously reported (Williams 2018*a*). One also observes small regions of the cloud throughout the measured volume that appear to be synchronous with the external modulation. These regions appear only for short periods of time and correspond to regions where the wave mode remains in the naturally occurring state whose dominant frequency mode happens to match the external modulation (Williams 2018*a*). As time passes, the volume of the wave that is synchronous with the external modulation reaches a steady value and remains relatively constant until the external modulation is discontinued. This final volume that is synchronous with an external modulation appears to be dependent on neutral gas pressure and the frequency of the modulation. In particular, it is observed that either a large or small volume of the cloud is synchronous with the external modulation and there are notable differences in these two cases. For the cases where a large volume of the cloud is synchronous with the external modulation, figure 2, there are large regions of the cloud volume that are synchronous with the external modulation but these regions exists in clusters

https://doi.org/10.1017/S0022377819000655 Published online by Cambridge University Press

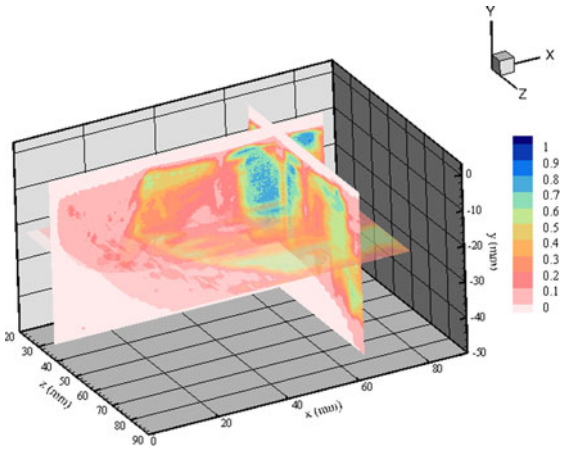

FIGURE 4. Slices through the experimental volume depicting the synchronization index with an external modulation of $f = 28$ at $p = 76$ mTorr.

throughout the cloud volume and the entire volume is not synchronous with the external modulation. This is seen in figures 2(*h*) and 4, where the synchronization index is plotted and elevated values represent the region of the wave volume that is synchronous with the external modulation. By contrast, in the cases where a small volume is of the cloud is observed to be synchronous, it is observed that the synchronous region is concentrated to a small volume of the wave directly under the modulation electrode, figure 3. When the external modulation is discontinued, it is clear that, as in the phase synchronization process, the loss of phase synchronization is not instantaneous, figures 2, 3(*i–p*) and the wave mode retains a memory of the previously applied external modulation. Here, it is observed that there is an immediate loss of phase synchronization in the region of the wave mode nearest the modulation electrode but the remaining wave volume behaves as if the external modulation was still present. As time passes, the region of the wave that retains this memory of the external modulation decreases as the wave volume near the electrode that immediately returned to natural wave mode expands until the entire wave mode exhibits the characteristics that are associated with the natural wave mode. This loss of phase synchronization happens behind a propagating desynchronization front that travels at a slower speed than the phase velocity of the wave. This desynchronization front exhibits the same characteristics as the synchronization front identified previously, namely that speed of this desynchronization front is slower than the phase velocity of the wave. Taken together, this suggests that the phase synchronization and desynchronization processes are dependent on the local plasma conditions which provide the coupling between the source of the external modulation and the dust cloud.

The behaviour of the synchronization and desynchronization fronts are better seen in figure 5(*a*), where the synchronization index along a vertical slice at $x = 54.59$ mm through the dust cloud immediately below the modulation electrode located at $y = 1.06$ mm is plotted as a function of time when a modulation frequency of 28 Hz is applied from $t = 8.5$ to 11.5 s. After the onset of the modulation, one observes a slight delay before the synchronization index suddenly increases, indicating the onset of the wave mode becoming synchronous with the external modulation. By tracking

https://doi.org/10.1017/S0022377819000655 Published online by Cambridge University Press

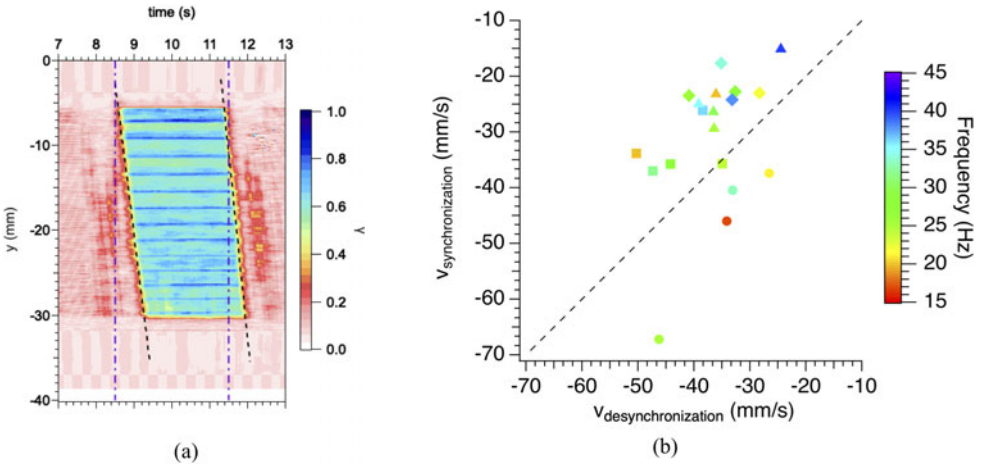

FIGURE 5. (*a*) Space–time plot showing the spatio-temporal evolution of the synchronization index, γ, along the vertical slice at $x = 54.59$ mm through the dust cloud immediately below the modulation electrode located at $y = 1.06$ mm as a modulation frequency of 28 Hz is applied at a pressure of 76 mTorr from $t = 8.5$ to 11.5 s. The black, dashed line indicates the propagation of the synchronization and desynchronization fronts, while the purple dash-dot line indicates when the modulation was applied. (*b*) Plot of the velocity of the synchronization front as a function of the velocity of the desynchronization front for $p = 61$ (solid circles), 76 (solid squares), 90 (solid triangles) and 106 (solid diamonds) mTorr. The black, dashed line indicates where the synchronization and desynchronization fronts would have the same speed.

this transition, it is possible to track the evolution of the synchronization front as it moves through the cloud, indicated by the left black, dashed line. Further, by extending the drive cycle when performing the analysis of the data, one also observes the clear existence of a desynchronization front, indicated by the right black, dashed line, behind which the wave mode returns to the naturally occurring wave mode. This transition occurs when there is a sudden drop in the synchronization index, indicating that the wave mode is no longer synchronous with the external modulation. This desynchronization front is also observed to travel at a speed that is slower than the phase velocity of the wave.

Figure 5(*b*) depicts the speed of the synchronization front as a function of the speed of the desynchronization front. Here, it is observed that, with the exception of the lowest pressure case, the speed of the synchronization front is generally slightly greater than the desynchronization front. In previous studies, the model of the van der Pol oscillator has been applied to model the phase synchronization of the dust acoustic wave (Menzel, Arp & Piel 2011*a*). This would suggest that coupling between dust grains may be different when looking at the phase synchronization and desynchronization process. Further, it appears the speeds of the synchronization and desynchronization fronts do not exhibit any dependence on the modulation frequency but both tend to decrease with increasing neutral gas pressures. This suggests that the dominant mechanism for the observed decrease in the speed of the synchronization front is the change in damping due to the higher collisionality with increasing neutral gas pressure. These observations provide a fingerprint that could be used to identify the physical mechanism responsible for the phase synchronization and desynchronization in this system but additional study is needed.

https://doi.org/10.1017/S0022377819000655 Published online by Cambridge University Press

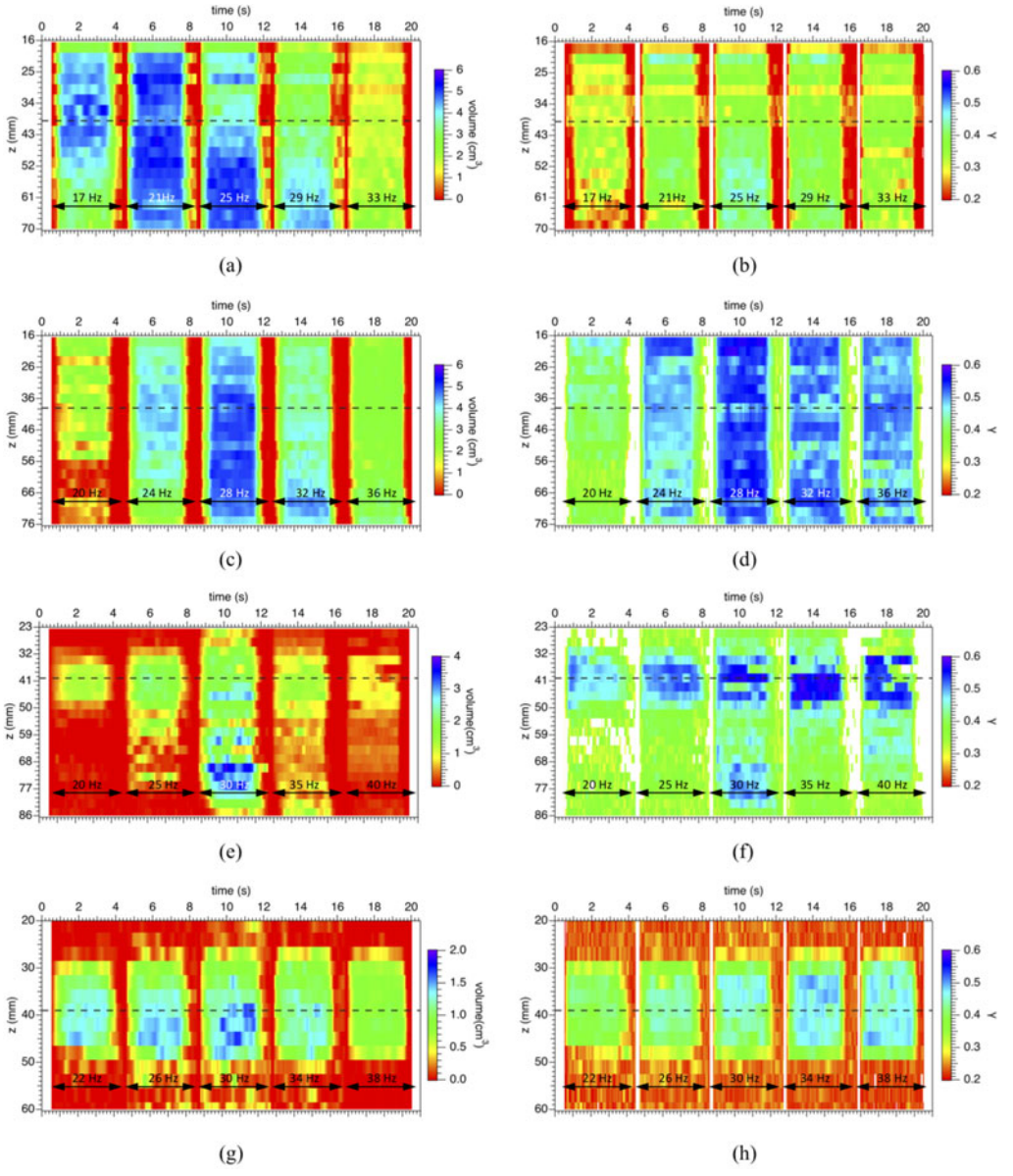

FIGURE 6. Space–time plot showing the spatio-temporal evolution of the (*a*,*c*,*e*,*g*) volume of the wave that is synchronous with the external modulation and (*b*,*d*,*f*,*h*) average synchronization index at each slice of the imaged cloud for $p = (a, b)$ 60, (*c*,*d*) 76, (*e*,*f*) 90 and (*g*,*h*) 106 mTorr. The black, dashed line indicates the location of the modulation electrode.

The volumetric nature of the phase synchronization is also seen in figure 6, where the (*a*,*c*,*e*,*g*) wave volume that is synchronous with the external modulation and (*b*,*d*,*f*,*h*) the average synchronization index are plotted as a function of time at each slice of the imaged cloud for the different pressures examined. Here, it is observed that the volume of the cloud that is synchronous and the average value

https://doi.org/10.1017/S0022377819000655 Published online by Cambridge University Press

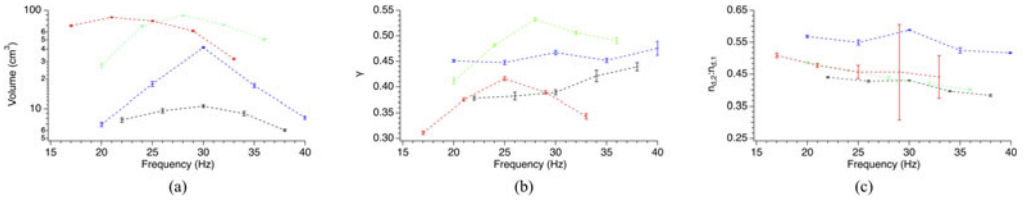

FIGURE 7. Plot of the (*a*) wave volume synchronous with an external modulation, (*b*) average synchronization index over the synchronized volume and (*c*) the nonlinearity in the wave as a function of the modulation frequency for $(p) = 61$ (black), 76 (blue), 90 (green) and 106 (red) mTorr.

of the synchronization index are a function of the spatial location, frequency of the external modulation and the neutral gas pressure. In particular, the entire volume of the cloud that is measurable is synchronous with the external drive at lower neutral gas pressures. As the pressure increases, the volume of the cloud that is synchronous with the external modulation becomes smaller and concentrated below the modulation electrode. Further, it is observed that these quantities also depend on the frequency of the external modulation. This is particularly clear at $p = 90$ mTorr, figure 5(*e*,*f*), where the wave volume of the cloud that is synchronous initially increases with modulation frequency before decreasing. It is also observed that the volume that is synchronous is concentrated in the region below the modulation electrode at the extreme edges of the range of frequencies.

The global properties of the synchronous wave mode are plotted as a function of the modulation frequency in figure 7. The total volume of the wave that is synchronous with the external modulation is plotted in figure 7(*a*), where it is observed that a large volume of the wave is observed to be synchronous at lower values of neutral gas pressure and that the volume that is synchronous decreases with increasing neutral gas pressure. Further, it is also observed that the volume of the wave that is synchronous initially increases with modulation frequency before reaching a peak value and then decreasing with modulation frequency. A similar trend is observed in the average synchronization index, figure 7(*b*), when a large volume of the cloud is synchronous with the external modulation. However, in the cases where a smaller volume of the wave is observed to be synchronous with the external modulation, the synchronization index tends to increase with modulation frequency. It is not presently clear why this might be the case but is a question to examine in the future. Finally, the nonlinearity of the wave that is synchronous with the external modulation is seen in figure 7(*c*). Here, the nonlinearity in the wave mode is quantified by fitting the amplitude of the driven wave to the sum of two sine waves, one at the modulation frequency and one at the first harmonic of the modulation frequency. The nonlinearity is then defined as the ratio of the amplitude of the first harmonic of the modulation frequency, $n_{d,2}$ to the amplitude of the modulation frequency, $n_{d,1}$ (Merlino 2012; Williams 2016). It is observed that the nonlinearity generally decreases with increasing frequency, suggesting that, while nonlinearity is required for phase synchronization, the specific measure of the nonlinearity is not critical. Taken together, these measurements provide insight and a potential signature for the physical mechanism that is responsible for the phase synchronization and desynchronization process, although it is not clear what this mechanism is at present.

https://doi.org/10.1017/S0022377819000655 Published online by Cambridge University Press

5. Conclusions

To summarize, we have presented a time-resolved measurement depicting the volumetric nature of the phase synchronization of a self-excited dust acoustic wave to an external modulation and the relaxation from the driven wave mode back to the naturally occurring wave mode (desynchronization) in a rf discharge over a range of neural gas pressures. Phase synchronization and desynchronization of the wave mode with an external modulation were observed to occur behind a propagating synchronization/desynchronization front that travels at a slower speed than the phase velocity of the wave and the speed of this synchronization front decreases with increasing neutral gas pressure. It is also observed that volume of the wave that is synchronous depends on the frequency of the external modulation and the neutral gas pressure.

REFERENCES

AVINASH, K. 2015 Theory of correlation effects in dusty plasmas. *Phys. Plasmas* **22** (3), 033701.

CHANG, M.-C., TENG, L.-W. & LIN, I. 2012 Micro-origin of no-trough trapping in self-excited nonlinear dust acoustic waves. *Phys. Rev.* E **85** (4), 046410.

COUËDEL, L., ZHDANOV, S., NOSENKO, V., IVLEV, A. V., THOMAS, H. M. & MORFILL, G. E. 2014 Synchronization of particle motion induced by mode coupling in a two-dimensional plasma crystal. *Phys. Rev.* E **89** (5), 053108.

DAVLETOV, A. E., YERIMBETOVA, L. T., ARKHIPOV, Y. V., MUKHAMETKARIMOV, Y. S., KISSAN, A. & TKACHENKO, I. M. 2018 Dust particles of finite dimensions in complex plasmas: thermodynamics and dust-acoustic wave dispersion. *J. Plasma Phys.* **84** (4), 4315.

FLANAGAN, T. M. & GOREE, J. 2011 Development of nonlinearity in a growing self-excited dust-density wave. *Phys. Plasmas* **18** (1), 013705.

HEINRICH, J. R., KIM, S. H., MEYER, J. K. & MERLINO, R. L. 2011 Experimental quiescent drifting dusty plasmas and temporal dust acoustic wave growth. *Phys. Plasmas* **18** (11), 113706.

KILLER, C. & MELZER, A. 2014 Global coherence of dust density waves. *Phys. Plasmas* **21** (6), 063703.

LIAO, C.-T., TENG, L.-W., TSAI, C.-Y., IO, C.-W. & LIN, I. 2008 Lagrangian–Eulerian micromotion and wave heating in nonlinear self-excited dust-acoustic waves. *Phys. Rev. Lett.* **100** (18), 185004.

LIU, B., GOREE, J., FLANAGAN, T. M., SEN, A., TIWARI, S. K., GANGULI, G. & CRABTREE, C. 2018 Experimental observation of cnoidal waveform of nonlinear dust acoustic waves. *Phys. Plasmas* **25** (11), 113701.

MAZA, D., VALLONE, A., MANCINI, H. & BOCCALETTI, S. 2000 Experimental phase synchronization of a chaotic convective flow. *Phys. Rev. Lett.* **85** (26), 5567–5570.

MENZEL, K. O., ARP, O. & PIEL, A. 2011*a* Chain of coupled van der Pol oscillators as model system for density waves in dusty plasmas. *Phys. Rev.* E **84** (1), 016405.

MENZEL, K. O., ARP, O. & PIEL, A. 2011*b* Frequency clusters and defect structures in nonlinear dust-density waves under microgravity conditions. *Phys. Rev.* E **83** (1), 016402.

MERLINO, RL. 2012 Second-order dust acoustic wave theory. *Phys. Scr.* **85**, 035506.

MERLINO, R. L. 2014 25 years of dust acoustic waves. *J. Plasma Phys.* **80** (6), 773–786.

NOSENKO, V., ZHDANOV, S. K., KIM, S. H., HEINRICH, J., MERLINO, R. L. & MORFILL, G. E. 2009 Measurements of the power spectrum and dispersion relation of self-excited dust acoustic waves. *Europhys. Lett.* **88** (6), 65001.

PIKOVSKY, A., ROSENBLUM, M. & KURTHS, J. 2001 *Synchronization*. Cambridge University Press.

PILCH, I., REICHSTEIN, T. & PIEL, A. 2009 Synchronization of dust density waves in anodic plasmas. *Phys. Plasmas* **16** (12), 123709.

ROSENBERG, M., THOMAS, E. JR & MERLINO, R. L. 2008 A note on dust wave excitation in a plasma with warm dust: comparison with experiment. *Phys. Plasmas* **15** (7), 073701.

https://doi.org/10.1017/S0022377819000655 Published online by Cambridge University Press

ROSENBLUM, M. G., PIKOVSKY, A. S. & KURTHS, J. 2004 Synchronization approach to analysis of biological systems. *World Scientific* **04** (01), L53–L62.

RUHUNUSIRI, W. D. S. & GOREE, J. 2012 Synchronization mechanism and Arnold tongues for dust density waves. *Phys. Rev.* E **85** (4), 046401.

RUHUNUSIRI, W. D. S. & GOREE, J. 2014 Dispersion relations for the dust-acoustic wave under experimental conditions. *Phys. Plasmas* **21** (5), 053702.

TADSEN, B., GREINER, F., GROTH, S. & PIEL, A. 2015 Self-excited dust-acoustic waves in an electron-depleted nanodusty plasma. *Phys. Plasmas* **22** (11), 113701.

TADSEN, B., GREINER, F. & PIEL, A. 2017 On the amplitude of dust-density waves in inhomogeneous dusty plasmas. *Phys. Plasmas* **24** (3), 033704.

TASS, P., ROSENBLUM, M. G., WEULE, J., KURTHS, J., PIKOVSKY, A., VOLKMANN, J., SCHNITZLER, A. & FREUND, H. J. 1998 Detection of n:m phase locking from noisy data: application to magnetoencephalography. *Phys. Rev. Lett.* **81** (15), 3291–3294.

TENG, L.-W., CHANG, M.-C., TSENG, Y.-P. & LIN, I. 2009 Wave-particle dynamics of wave breaking in the self-excited dust acoustic wave. *Phys. Rev. Lett.* **103** (24), 245005.

THOMAS, E. JR 2006 Measurements of spatially growing dust acoustic waves in a DC glow discharge plasma. *Phys. Plasmas* **13** (4), 042107.

THOMAS, E. JR, FISHER, R. & MERLINO, R. L. 2007 Observations of dust acoustic waves driven at high frequencies: finite dust temperature effects and wave interference. *Phys. Plasmas* **14** (12), 123701.

TICOS, C. M., EPAMINONDAS ROSA, J., PARDO, W. B., WALKENSTEIN, J. A. & MONTI, M. 2000 Experimental real-time phase synchronization of a paced chaotic plasma discharge. *Phys. Rev. Lett.* **85** (14), 2929–2932.

TROTTENBERG, T., BLOCK, D. & PIEL, A. 2006 Dust confinement and dust-acoustic waves in weakly magnetized anodic plasmas. *Phys. Plasmas* **13** (4), 042105.

TSAI, Y.-Y., CHANG, M.-C. & LIN, I. 2014 Dynamical behaviors of nonlinear dust acoustic waves: from plane waves to dust acoustic wave turbulence. *J. Plasma Phys.* **80** (6), 809–816.

WILLIAMS, J. 2013 Spatial evolution of the dust-acoustic wave. *Plasma Science, IEEE Transactions on* **41** (4), 788–793.

WILLIAMS, J. 2016 Application of the Hilbert Transform to measure the nonlinearity in the driven dust acoustic wave. *Plasma Science, IEEE Transactions on* **44**, 562–567.

WILLIAMS, J. 2018*a* Synchronization of the dust acoustic wave in an RF and a DC discharge plasma. *Plasma Science, IEEE Transactions on* **46** (4), 806–814.

WILLIAMS, J. D. 2014*a* Evolution of frequency clusters in the naturally occurring dust acoustic wave. *Phys. Rev.* E **89** (2), 023105.

WILLIAMS, J. D. 2014*b* Time-resolved measurement of global synchronization in the dust acoustic wave. *Phys. Rev.* E **90** (4), 043103.

WILLIAMS, J. D. 2018*b* Volumetric measurement of synchronization of the dust acoustic wave with an external modulation. *AIP Conference Proceedings* **1925** (1), 020011.

WILLIAMS, J. D. & SNIPES, E. K. 2010 Measurements of the dust temperature in the dispersion relation of the dust acoustic wave. *Plasma Science, IEEE Transactions on* **38** (4), 847–851.

YAROSHENKO, V. V., KHRAPAK, S. A., PUSTYLNIK, M. Y., THOMAS, H. M., JAISWAL, S., LIPAEV, A. M., USACHEV, A. D., PETROV, O. F. & FORTOV, V. E. 2019 Excitation of low-frequency dust density waves in flowing complex plasmas. *Phys. Plasmas* **26** (5), 053702.